FREE CONVECTION HEAT TRANSFER FLOW IN A VERTICAL CONICAL THROUGH POROUS MEDIUM WITH RADIATION

[#1] Dr. M.Nagaraju , [#2] Shaik Sharmila,
[#2] Prof. R.Siva Prasad

[#1] Lecturer in Mathematics, S.Y.T.R Govt. Degree College,
Madakasira, Ananthapuramu(Dist.)
[#2]Department of Mathematics, Sri Krishnadevaraya University,
Ananthapuramu-515003, A.P., India

_____

ABSTRACT:

In this paper, we concentrate on the study of heat transfer by free Convection in a saturated porous medium including radiation confined in a vertical conical annular porous medium

KEYWORDS: Heat transfer, Rayleigh number, Nusselt number, Radiation Parameter

_____

1. INTRODUCTION

Study of buoyancy induced convection flow and heat transfer in fluid saturated porous medium has recently attracted considerable interest because of a number of important energy related engineering and geophysical applications such as thermal insulation of buildings, geothermal engineering enhanced recovery of petroleum resources, filtration processes, ground water pollution and sensible heat storage beds.

Free convection about a vertical flat plate embedded in a porous medium at high Rayleigh numbers was analyzed by Cheng and Minkowycz (1), Na and Pop (2) studied free convection flow past a vertical flat plate maintained at a non-uniform surface temperature embedded in a saturated porous medium and presented numerical results by employing a two-port finite difference method. Gorla and Zinalabedinin (3) studied the free convection from a vertical plate embedded in saturated porous medium.

Heat transfer by mixed convention in laminar boundary layer flow has been analyzed extensively for flat plate geometry in saturated porous media in vertical, horizontal and inclined orientations. Typical studies can be found, for example in (11-14).

In this chapter, we concentrate on the study of heat transfer by free convection in a saturated porous medium including radiation confined in a vertical conical annular porous medium. In this study, Finite Element method (FEM) has been used to solve the governing partial differential equations. Results are presented interms of average Nusselt number ($\overline{Nu}$), streamlines and Isothermal lines for Various values of Rayleigh number (R_a), Cone angle (c_A), Radius ratio (R_r) and Radiation parameter (R_d).

_____

2. MATHEMATICAL FORMULATIONS

A vertical annular cone of inner radius r_1 and outer radius r_0 as depicted by schematic diagram as in figure is considered to investigate the heat transfer behaviour. The co-ordinate system in chosen such that the γ-axis points towards the width z axis towards the height of the come respectively. Because of the annular nature, two important parameters emerge which are Cone angle (c_A) and Radius ratio (R_r) of the annular. They are defined as

$$c_A = \frac{H_t}{r_0 - r_i} \qquad\qquad R_r = \frac{r_0 - r_i}{r_i}$$

where H_t is the height of the cone.

The inner surface of the cone is maintained at isothermal temperature T_n and outer surface is at ambient temperature T_∞. It may be noted that, due to axisymmetry, a section of the annulus is sufficient for analysis purpose.

We assume that the flow inside the porous medium is assumed to obey Darcy law and there is no phase change of fluid. The properties of the fluid and porous medium are homogeneous, isotropic and constant except for variation of fluid density with temperature. The fluid and porous medium are in thermal equilibrium.

The continuity equation

$$\frac{\partial(ru)}{\partial r} + \frac{\partial p}{\partial r} = 0 \tag{2.1}$$

The velocity in r and z directions can be described by Darcy law as velocity in horizontal direction

$$u = \frac{-k}{\mu}\frac{\partial p}{\partial r} = 0$$

Velocity in vertical direction

$$w = \frac{-k}{\mu}\left(\frac{\partial p}{\partial z} + \rho g\right)$$

The permeability k of porous medium can be expressed as Bejan [23]

$$k = \frac{D_p^2\phi^3}{180(1-\phi)^2}$$

The variation of density with respect to temperature can be described by Boussinesq approximation as

$$\rho = \rho_\alpha[1 - \beta_T(T - T_\infty)] \tag{2.2}$$

The Momentum equation

$$\frac{\partial w}{\partial r} - \frac{\partial u}{\partial z} = \frac{gk\beta}{v}\frac{\partial T}{\partial r} \tag{2.3}$$

The energy equation

$$u\frac{\partial T}{\partial r} + w\frac{\partial T}{\partial r} = \alpha\left[\frac{1}{r}\frac{\partial}{\partial r}\left(r\frac{\partial T}{\partial r}\right) + \frac{\partial^2 T}{\partial z^2}\right] - \frac{1}{\rho C_P} - \frac{1}{r}\frac{\partial}{\partial r}(rq_r) \tag{.2.4}$$

The last term in the R.H.S of the equation (2.2.4) represents the radiation effect.

The continuity equation (2.2.1) can be satisfied by introducing the stream function ψ as

$$u = \frac{-1}{r}\frac{\partial \psi}{\partial z}, \qquad\qquad w = \frac{-1}{r}\frac{\partial \psi}{\partial r} \qquad\qquad (2.5)$$

Rosseland approximation for radiation is [23]

$$q_r = \frac{4n^2\sigma}{3\beta_R}\frac{\partial T^4}{\partial r}$$

The corresponding dimensional boundary conditions we

$$
\left.
\begin{array}{llll}
\text{at} & r = r_i, & T = T_w, & \psi = 0 \\
\text{at} & r = r_0, & T = T_\infty, & \psi = 0 \\
& & & (\text{except at } z = 0)
\end{array}
\right\} \qquad (2.6)
$$

The new parameters arising due to cylindrical co-ordinates system are

Non-dimensional Radius, $\bar{r} = \dfrac{r}{L}$,   Non-dimensional height $\bar{z} = \dfrac{z}{L}$

Non-dimensional stream faction $\bar{\psi} = \dfrac{\psi}{\alpha L}$,Non-dimensional temperature $\bar{T} = \dfrac{(T - T_\infty)}{(T_w - T_\infty)}$

Rayleigh number $R_a = \dfrac{g\beta_T \Delta T K L}{\upsilon\alpha}$, Radiation parameter $R_d = \dfrac{4\sigma n^2 T_c^3}{\beta_R K_S}$

The non-dimensional equations for the heat transfer in vertical cone are
The Momentum equation

$$\frac{\partial^2 \bar{\psi}}{\partial \bar{z}^2} + \bar{r}\left(\frac{1}{r}\frac{\partial \bar{\psi}}{\partial \bar{r}}\right) = \bar{r}R_a\frac{\partial \bar{T}}{\partial \bar{r}} \qquad (2.7)$$

The Energy equation

$$\frac{1}{r}\left[\frac{\partial \bar{\psi}}{\partial \bar{r}}\frac{\partial \bar{T}}{\partial \bar{z}} - \frac{\partial \bar{\psi}}{\partial \bar{z}}\frac{\partial \bar{T}}{\partial \bar{r}}\right] = \left[\frac{1}{r}\frac{\partial}{\partial \bar{r}}\left(\left(1 + \frac{4R_d}{2}\right)\bar{r}\frac{\partial \bar{T}}{\partial \bar{r}}\right) + \frac{\partial^2 \bar{T}}{\partial \bar{z}^2}\right] \qquad (2.8)$$

The corresponding non-dimensional boundary conditions are

$$
\left.
\begin{array}{llll}
\text{at} & \bar{r} = \bar{r}_i, & \bar{T} = 1, & \bar{\psi} = 0 \\
\text{at} & \bar{r} = \bar{r}_0, & \bar{T} = 0, & \bar{\psi} = 0
\end{array}
\right\} \qquad (2.9)
$$

3 SOLUTION OF GOVERNING EQUATIONS:-

Applying Garerkin method to momentum equation (2.2.9) yields:

$$\{R^e\} = -\int_A N^T\left(\frac{\partial^2 \bar{\psi}}{\partial Z^{-2}} + \bar{r}\frac{\partial}{\partial \bar{r}}\left(\frac{1}{\bar{r}}\frac{\partial \bar{\psi}}{\partial \bar{r}}\right) - \bar{r}Ra\frac{\partial \bar{T}}{\partial \bar{r}}\right)dV \qquad (3.1)$$

$$\{R^e\} = -\int_A N^T\left(\frac{\partial^2 \bar{\psi}}{\partial Z^{-2}} + \bar{r}\frac{\partial}{\partial \bar{r}}\left(\frac{1}{\bar{r}}\frac{\partial \bar{\psi}}{\partial \bar{r}}\right) - \bar{r}Ra\frac{\partial \bar{T}}{\partial \bar{r}}\right)2\pi\bar{r}dA \qquad (3.2)$$

where R^e is the residue. Considering individual terms of equation (2.3.2)

$$\frac{\partial}{\partial \bar{r}}\left([N^T]\frac{\partial \bar{\psi}}{\partial \bar{r}}\right) = \left([N^T]\frac{\partial^2 \bar{\psi}}{\partial r^{-2}}\right) + \frac{\partial[N]^T}{\partial \bar{r}}\frac{\partial \bar{\psi}}{\partial \bar{r}} \qquad (3.3)$$

Thus

$$\int_A N^T \frac{\partial^2 \overline{\psi}}{\partial r^{-2}} dA = \int_A \frac{\partial}{\partial \overline{r}} \left([N^T] \frac{\partial \overline{\psi}}{\partial \overline{r}} \right) 2\pi \overline{r} dA - \int_A \frac{\partial [N]^T}{\partial \overline{r}} \frac{\partial \overline{\psi}}{\partial \overline{r}} \tag{3.4}$$

The first term on RHS of equation (3.4) can be transformed into surface by the application of Greens theorem and leads to inter-element requirement at boundaries of an element. The boundary conditions are incorporated in the force vector.

Let us consider that the variable to be determined in the triangular area as "T". The polynomial function for "T" can be expressed as

$$T = \alpha_1 + \alpha_2 r + \alpha_3 Z \tag{3.5}$$

The variable T has the value T_i, T_j, T_k at the nodal position i, j and k of the element. The r and Z coordinates at these points are r_i, r_j, r_k and Z_i, Z_j, Z_k respectively.

Since $T = N_i T_i + N_j T_j + N_k T_k$ (3.6)

where $N_i N_j, N_k$ are shape functions given by

$$N_m = \frac{a_m + b_m r + c_m Z}{2A} \tag{3.7}$$

Making use of (3.7) gives

$$\int_A N^T \frac{\partial^2 \overline{T}}{\partial Z^{-2}} 2\pi \overline{r} dA = -\int_A \frac{\partial N^T}{\partial \overline{r}} \frac{\partial N}{\partial \overline{r}} \begin{Bmatrix} \overline{\psi}_1 \\ \overline{\psi}_2 \\ \overline{\psi}_3 \end{Bmatrix} dA \tag{3.8}$$

Substitution of (3.7) into (3.8) gives

$$= \frac{1}{(2A)^2} \int_A \begin{bmatrix} b_1 \\ b_2 \\ b_3 \end{bmatrix} [b_1 b_2 b_3] \begin{Bmatrix} \overline{\psi}_1 \\ \overline{\psi}_2 \\ \overline{\psi}_3 \end{Bmatrix} 2\pi \overline{r} dA$$

$$= \frac{2\pi \overline{R}}{4A} \begin{bmatrix} b_1^2 & b_1 b_2 & b_1 b_3 \\ b_1 b_2 & b_2^2 & b_2 b_3 \\ b_1 b_3 & b_2 b_3 & b_3^2 \end{bmatrix} \begin{Bmatrix} \overline{\psi}_1 \\ \overline{\psi}_2 \\ \overline{\psi}_3 \end{Bmatrix} \tag{3.9}$$

Similarly $\int_A N^T \frac{\partial^2 \overline{\psi}}{\partial Z^{-2}} 2\pi \overline{r} dA = \frac{-2\pi \overline{R}}{4A} \begin{bmatrix} c_1^2 & c_1 c_2 & c_1 c_3 \\ c_1 c_2 & c_2^2 & c_2 c_3 \\ c_1 c_3 & c_2 c_3 & c_3^2 \end{bmatrix} \begin{Bmatrix} \overline{\psi}_1 \\ \overline{\psi}_2 \\ \overline{\psi}_3 \end{Bmatrix}$ (3.10)

The third term of equation (3.2)

$$\int_A N^T \overline{r} Ra \frac{\partial \overline{T}}{\partial \overline{r}} 2\pi \overline{r} dA = Ra \int_A N^T \overline{r} \frac{\partial \overline{T}}{\partial \overline{r}} 2\pi \overline{r} dA \tag{3.11}$$

Since $M_1 = N_1$, $M_2 = N_2$, $M_3 = N_3$

Where M_1, M_2 and M_3 are the area ratios of the Δ^{le} and N_1, N_2 and N_3 are the shape functions.

Replacing the shape function in the above equation (3.11) gives

$$\int_A N^T \overline{r} Ra \frac{\partial \overline{T}}{\partial \overline{r}} 2\pi \overline{r} dA = \overline{r} Ra \int_A \begin{bmatrix} M_1 \\ M_2 \\ M_3 \end{bmatrix} \frac{\partial (N)}{\partial \overline{r}} \begin{bmatrix} \overline{T}_1 \\ \overline{T}_2 \\ \overline{T}_3 \end{bmatrix} 2\pi \overline{r} dA \tag{3.12}$$

$$= Ra \frac{A}{3} \begin{bmatrix} 1 \\ 1 \\ 1 \end{bmatrix} \frac{2\pi R^{-2}}{2A} [b_1 + b_2 + b_3] \begin{bmatrix} \overline{T}_1 \\ \overline{T}_2 \\ \overline{T}_3 \end{bmatrix}$$

$$= \frac{2\pi R^{-2} Ra}{2A} \begin{Bmatrix} b_1\overline{T}_1 + b_2\overline{T}_2 + b_3\overline{T}_3 \\ b_1\overline{T}_1 + b_2\overline{T}_2 + b_3\overline{T}_3 \\ b_1\overline{T}_1 + b_2\overline{T}_2 + b_3\overline{T}_3 \end{Bmatrix} \tag{3.13}$$

Now Momentum equation leads to

$$\frac{2\pi \overline{R}}{4A} \left\{ \begin{bmatrix} b^2 & b_1 b_2 & b_1 b_3 \\ b_1 b_2 & b_2^2 & b_2 b_3 \\ b_1 b_3 & b_2 b_3 & b_3^2 \end{bmatrix} + \begin{bmatrix} c_1^2 & c_1 c_2 & c_1 c_3 \\ c_1 c_2 & c_2^2 & c_2 c_3 \\ c_1 c_3 & c_2 c_3 & c_3^2 \end{bmatrix} \right\} \begin{Bmatrix} \overline{\psi}_1 \\ \overline{\psi}_2 \\ \overline{\psi}_3 \end{Bmatrix}$$

$$+ \frac{2\pi R^{-2} Ra}{6} \begin{Bmatrix} b_1\overline{T}_1 + b_2\overline{T}_2 + b_3\overline{T}_3 \\ b_1\overline{T}_1 + b_2\overline{T}_2 + b_3\overline{T}_3 \\ b_1\overline{T}_1 + b_2\overline{T}_2 + b_3\overline{T}_3 \end{Bmatrix} = 0 \tag{3.14}$$

Which is in the form of stiffness matrix.

$$[K_s] \{\overline{\psi}\} = \{f\}$$

Similarly application of Galerkin method to energy equation (3.14) gives

$$\{R^e\} = -\int_A N^T \left[\frac{1}{\overline{r}} \left(\frac{\partial \overline{\psi}}{\partial \overline{r}} \frac{\partial \overline{T}}{\partial \overline{z}} - \frac{\partial \overline{\psi}}{\partial \overline{z}} \frac{\partial \overline{T}}{\partial \overline{r}} \right) \right] - \left[\frac{1}{r} \frac{\partial}{\partial \overline{r}} \left(\left(1 + \frac{4R_d}{3} \right) \overline{r} \frac{\partial \overline{T}}{\partial \overline{r}} + \frac{\partial^2 \overline{T}}{\partial \overline{z}^2} \right) \right] 2\pi \overline{r} dA \tag{3.15}$$

Considering the terms individually of the above equation (3.15)

$$\int_A [N]^T \frac{\partial \overline{\psi}}{\partial Z} \frac{\partial \overline{T}}{\partial \overline{r}} 2\pi dA = \int_A \begin{bmatrix} M_1 \\ M_2 \\ M_3 \end{bmatrix} \frac{d[N]}{d\overline{Z}} \{\overline{\psi}\} \frac{d[N]}{d\overline{r}} \{\overline{T}\} 2\pi \overline{r} dA$$

$$= \frac{2\pi A}{3} \times \frac{1}{4A^2} [c_1\overline{\psi}_1 + c_2\overline{\psi}_2 + c_3\overline{\psi}_3][b_1, b_2, b_3] \begin{bmatrix} \overline{T}_1 \\ \overline{T}_2 \\ \overline{T}_3 \end{bmatrix} \tag{.3.16}$$

$$= \frac{2\pi}{12A} \begin{Bmatrix} c_1\overline{\psi}_1 + c_2\overline{\psi}_2 + c_3\overline{\psi}_3 \\ c_1\overline{\psi}_1 + c_2\overline{\psi}_2 + c_3\overline{\psi}_3 \\ c_1\overline{\psi}_1 + c_2\overline{\psi}_2 + c_3\overline{\psi}_3 \end{Bmatrix} [b_1, b_2, b_3] \begin{bmatrix} \overline{T}_1 \\ \overline{T}_2 \\ \overline{T}_3 \end{bmatrix} \tag{3.17}$$

Following the same above procedure.

$$\int_A [N]^T \frac{\partial \overline{\psi}}{\partial \overline{r}} \frac{\partial \overline{T}}{\partial \overline{z}} 2\pi dA = \int_A \begin{bmatrix} M_1 \\ M_2 \\ M_3 \end{bmatrix} \frac{d[N]}{d\overline{r}} \{\overline{\psi}\} \frac{d[N]}{d\overline{z}} \{\overline{T}\} 2\pi dA$$

$$\int_A N^T \frac{\partial \overline{\psi}}{\partial \overline{r}} \frac{\partial \overline{T}}{\partial \overline{Z}} 2\pi dA = \frac{2\pi}{12A} \begin{Bmatrix} b_1\overline{\psi}_1 + b_2\overline{\psi}_2 + b_3\overline{\psi}_3 \\ b_1\overline{\psi}_1 + b_2\overline{\psi}_2 + b_3\overline{\psi}_3 \\ b_1\overline{\psi}_1 + b_2\overline{\psi}_2 + b_3\overline{\psi}_3 \end{Bmatrix} [c_1, c_2, c_3] \begin{bmatrix} \overline{T}_1 \\ \overline{T}_2 \\ \overline{T}_3 \end{bmatrix} \tag{3.18}$$

The remaining terms of Energy equation can be evaluated in similar fashion of Momentum equation gives

$$\int_A N^T \left[\frac{1}{\bar{r}} \frac{\partial}{\partial \bar{r}} \left(1 + \frac{4R_d}{3} \right) \right] 2\pi \bar{r} \, dA = \left[1 + \frac{4R_d}{3} \right] \frac{-2\pi\bar{R}}{4A} \begin{bmatrix} b_1^2 & b_1 b_2, & b_1 b_3 \\ b_1 b_2 & b_2^2 & b_2 b_3 \\ b_1 b_3 & , b_2 b_3 & b_3^2 \end{bmatrix} \begin{Bmatrix} \bar{T}_1 \\ \bar{T}_2 \\ \bar{T}_3 \end{Bmatrix} \quad (3.19)$$

$$\int_A N^T \left[\frac{\partial^2 \bar{T}}{\partial z^{-2}} \right] 2\pi\bar{r} \, dA = \frac{-2\pi\bar{R}}{4A} \begin{bmatrix} c_1^2 & c_1 c_2 & c_1 c_3 \\ c_1 c_2 & c_2^2 & c_2 c_3 \\ c_1 c_3 & c_2 c_3 & c_3^2 \end{bmatrix} \begin{Bmatrix} \bar{T}_1 \\ \bar{T}_2 \\ \bar{T}_3 \end{Bmatrix} \quad (3.20)$$

Thus the stiffness matrix of energy equation (3.14) is given by:

$$\left[\frac{2\pi}{12A} \begin{Bmatrix} c_1\bar{\psi}_1 + & c_2\bar{\psi}_2 + & c_3\bar{\psi}_3 \\ c_1\bar{\psi}_1 + & c_2\bar{\psi}_2 + & c_3\bar{\psi}_3 \\ c_1\bar{\psi}_1 + & c_2\bar{\psi}_2 + & c_3\bar{\psi}_3 \end{Bmatrix} [b_1, b_2, b_3] - \frac{2\pi}{12A} \begin{Bmatrix} b_1\bar{\psi}_1 + & b_2\bar{\psi}_2 + & b_3\bar{\psi}_3 \\ b_1\bar{\psi}_1 + & b_2\bar{\psi}_2 + & b_3\bar{\psi}_3 \\ b_1\bar{\psi}_1 + & b_2\bar{\psi}_2 + & b_3\bar{\psi}_3 \end{Bmatrix} [c_1, c_2, c_3] \right]$$

$$\begin{bmatrix} \bar{T}_1 \\ \bar{T}_2 \\ \bar{T}_3 \end{bmatrix} + \frac{2\pi\bar{R}}{4A} \left\{ \left\{ 1 + \frac{4R_d}{3} \right\} \begin{bmatrix} b_1^2 & b_1 b_2 & b_1 b_3 \\ b_1 b_2 & b_2^2 & b_2 b_3 \\ b_1 b_3 & b_2 b_3 & b_3^2 \end{bmatrix} \begin{bmatrix} \bar{T}_1 \\ \bar{T}_2 \\ \bar{T}_3 \end{bmatrix} + \begin{bmatrix} c_1^2 & c_1 c_2, & c_1 c_3 \\ c_1 c_2 & c_2^2 & c_2 c_3 \\ c_1 c_3 & , c_2 c_3 & c_3^2 \end{bmatrix} \begin{bmatrix} \bar{T}_1 \\ \bar{T}_2 \\ \bar{T}_3 \end{bmatrix} \right\}$$

$$+ \frac{2\pi A \in}{12\bar{r}} \left\{ \begin{bmatrix} 1 \\ 1 \\ 1 \end{bmatrix} [b_1\bar{\psi}_1 + b_2\bar{\psi}_2 + b_3\bar{\psi}_3]^2 + \begin{bmatrix} 1 \\ 1 \\ 1 \end{bmatrix} [c_1\bar{\psi}_1 + c_2\bar{\psi}_2 + c_3\bar{\psi}_3]^2 \right\} = 0 \quad (3.21)$$

4 RESULTS AND DISCUSSION:

Results are obtained in terms of the average Nusselt number ($\bar{N}u$) at hot wall for various parameters such as Rayleigh number (R_a), Cone angle (c_A) radiation parameter (R_d), and Radius ratio (R_r) when heat is supplied to vertical conical annulus.

The average Nusselt number ($\bar{N}u$), is given by $\bar{N}u = \int_0^{\bar{z}} \left(\frac{\partial \bar{T}}{\partial \bar{r}} \right)$

Fig (4.1) shows the streamlines and isothermal lines inside porous medium for various value of Cone angle (c_A) at $R_a = 50$, $R_r = 1$ and $R_d = 1$. The fluid gets heated up near hot wall and moves up towards the cold wall due to high buoyancy force and then return to hot wall of the vertical annular cone. The boundary layer thickness decrease with the increase of the Cone angle (c_A).

Fig (4.2) shows the streamlines and isothermal line distribution inside the porous medium for various values of Cone angle (c_A) at $R_a = 100$, $R_r = 1$, and $R_d = 1$. With increase of the Rayleigh number (R_a) the thickness of the boundary layer decreases relatively with the Fig (4.1) as expected.

Fig (4.3) shows the variation of average Nusselt number ($\bar{N}u$) at hot wall with respect to Rayleigh number (R_a) of the vertical annular cone for various values of Cone angle (c_A) at $R_r = 1$, $R_d = 1$. It is found that the average Nusselt number ($\bar{N}u$) increases with increase in Rayleigh number (R_a). It can be seen that the average Nusselt number ($\bar{N}u$) increases with increase in Cone Angle (c_A) for a given Rayleigh number (R_a). The difference between the

average Nusselt number at two different values of Cone angle (c_A) increases with Cone angle (c_A) for instance, the average Nusselt number ($\bar{Nu}$) increased by 11.4% when Cone angle (c_A) is increased from 15 to 45 Ra = 10. However the average Nusselt number ($\bar{Nu}$) increased by 13.8%, when Cone angle (c_A) is increased from 15 to 45 at   Ra = 100. This difference becomes more prominent as the Rayleigh number (R_a) increases for particular value of Cone angle (c_A).
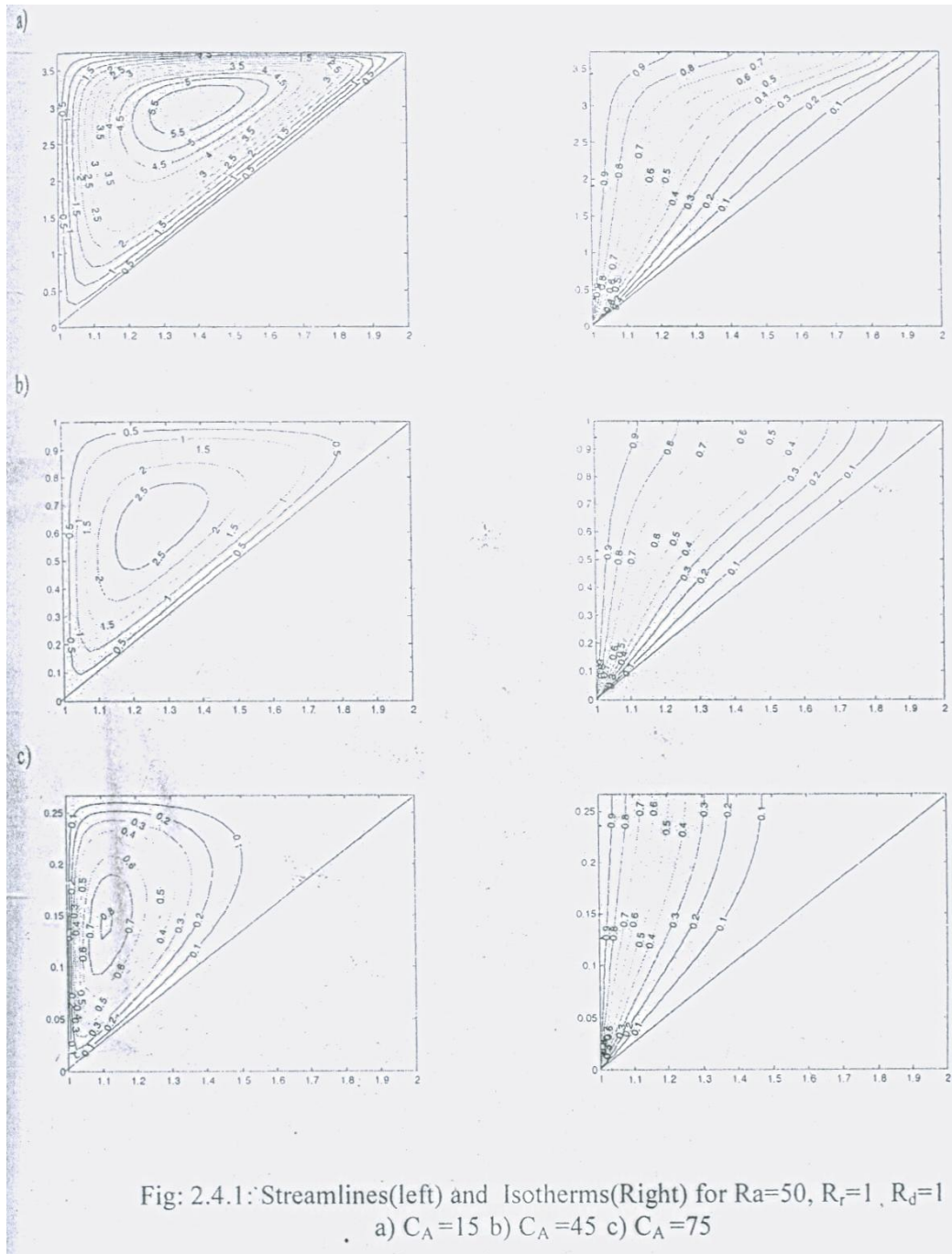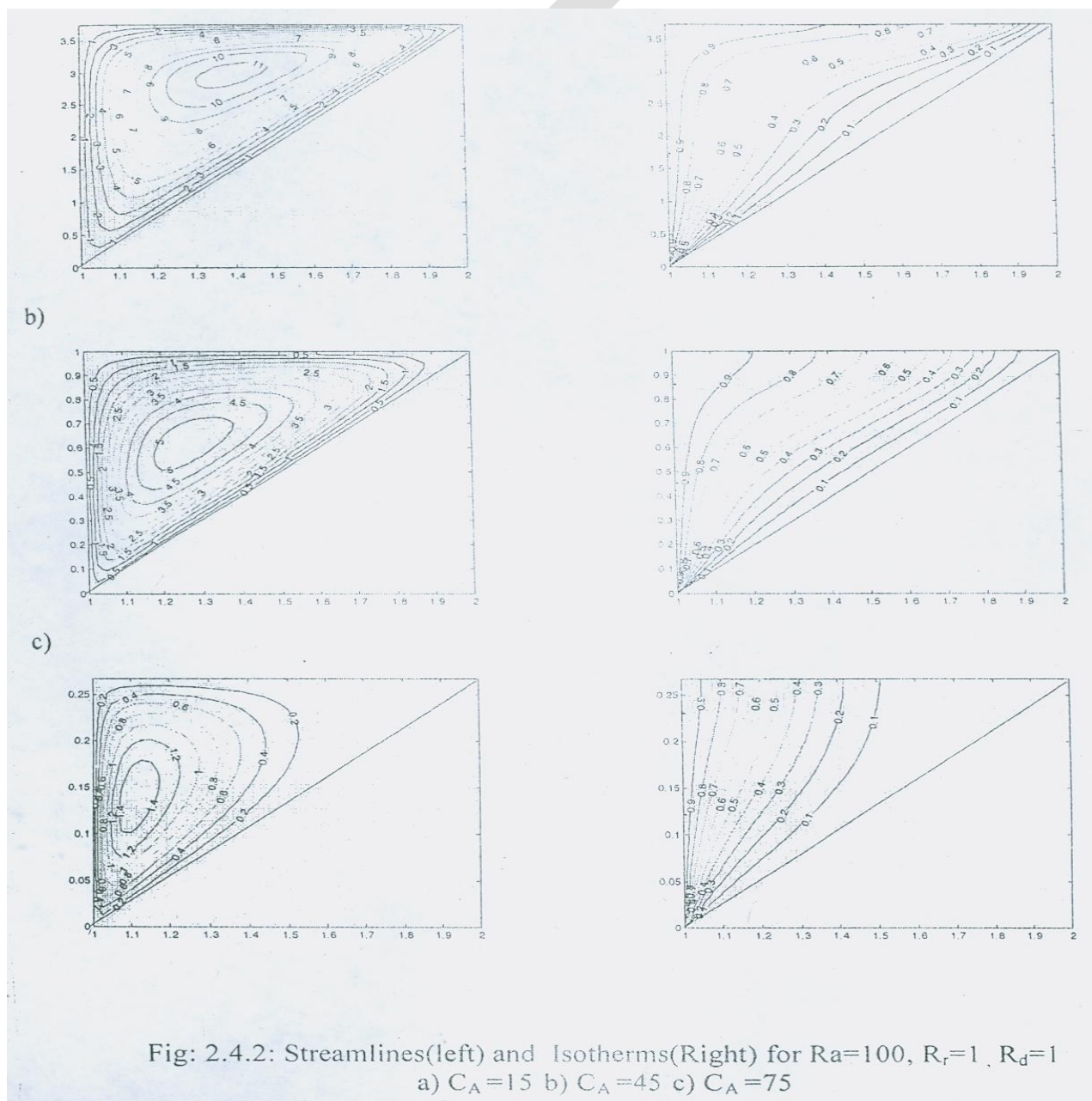

Fig: 2.4.1: Streamlines(left) and Isotherms(Right) for Ra=50, R_r=1, R_d=1
a) C_A =15 b) C_A =45 c) C_A =75

Fig (4.4) depicts the average Nusselt number ($\bar{Nu}$) at hot wall with respect to Rayleigh number (R_a), for various values of Radius ratio (R_r). This figure corresponds to the values c_A = 75, R_d = 1. It is found that the average Nusselt number ($\bar{Nu}$) increases with increase in Rayleigh number (R_a). It can be seen that the average Nusselt number ($\bar{Nu}$) increases with increase in Radius ratio (R_r). For a given Rayleigh number (R_a), the difference between the

average Nusselt number ($\overline{Nu}$) at two different values of Radius ratio (R_r) increase with increase in Radius ratio (R_r). For instance, the average Nusselt number ($\overline{Nu}$) increased by 56%, when Radius ratio (R_r) is increased from 1 to 5 at $R_a = 10$. However the average Nusselt number ($\overline{Nu}$) increased by 57% when Radius ratio (R_r) is increased from 1 to 5 at $R_a = 100$. This difference becomes more as the Rayleigh number (R_a) increases for particular value of Radius ratio (R_r).

Fig (4.5) shows the streamlines and isothermal lines inside the porous medium for various values of Radius ratio (R_r) at $R_a = 50$, $c_A = 15$ and $R_d = 1$. As the value of Radius ratio (R_r) increase the magnitude of the streamlines decreases. This is due to reasons that the increased Radius ratio (R_r) promotes the fluid movement due to the higher buoyancy force, which in turn allows the convection heat transfer at lower portion of the hot wall of the vertical angular cone. The thermal boundary layer thickness decreases as the Radius ratio (R_r) increases.
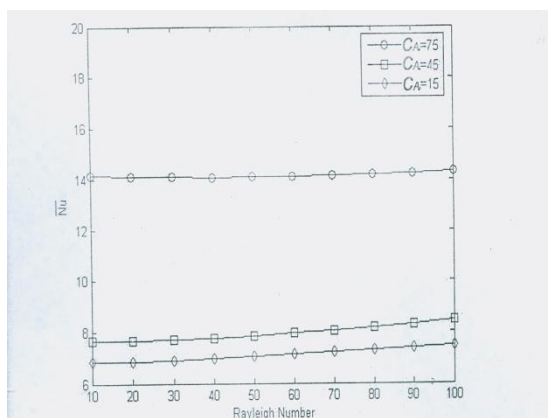

Fig: 2.4.2: Streamlines(left) and Isotherms(Right) for Ra=100, R_r=1 , R_d=1
a) C_A=15 b) C_A=45 c) C_A=75

Fig. 2.4.3 : $\overline{Nu}$ variations with Ra at hot surface for different values of C_A at $R_r=1$, $R_d=1$

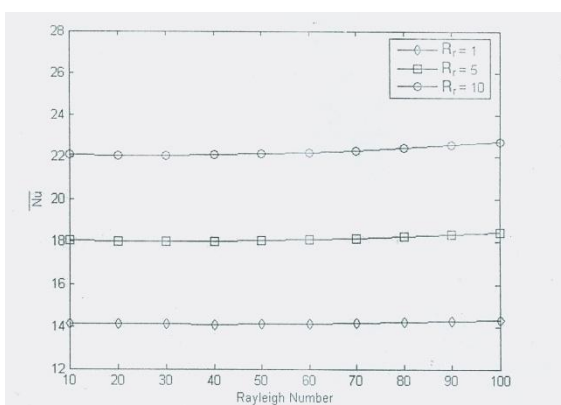Fig.2.4.4: $\overline{Nu}$ variations with Ra at hot surface for different values of R_r at $C_A=75$, $R_d=1$
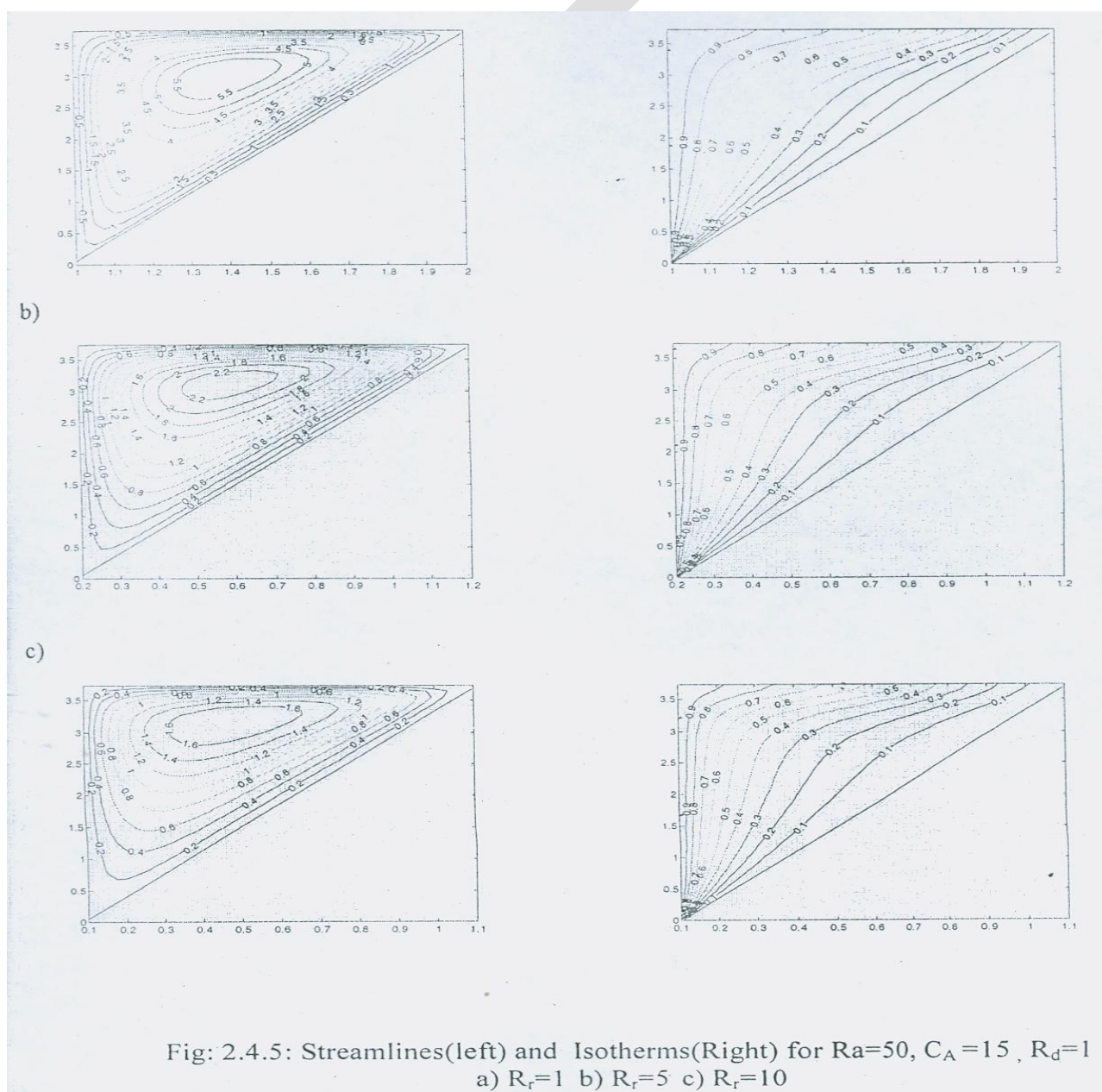

b)

c)

Fig: 2.4.5: Streamlines(left) and Isotherms(Right) for Ra=50, C_A =15 , R_d=1
a) R_r=1 b) R_r=5 c) R_r=10

Fig (4.6) shows the streamlines and isothermal lines inside the porous medium for various values of Radius ratio (R_r) at $R_a = 100$, $c_A = 15$ and $R_d = 1$. With comparison of the Fig (4.5) the boundary layer thickness of the Fig (2.4.6) decrease because of the increase of value of Rayleigh number ($R_a = 100$).

Fig:2.4.6: Streamlines(left) and Isotherms(Right) for Ra=100, C_A =15 , R_d=1
a) R_r=1 b) R_r=5 c) R_r=10
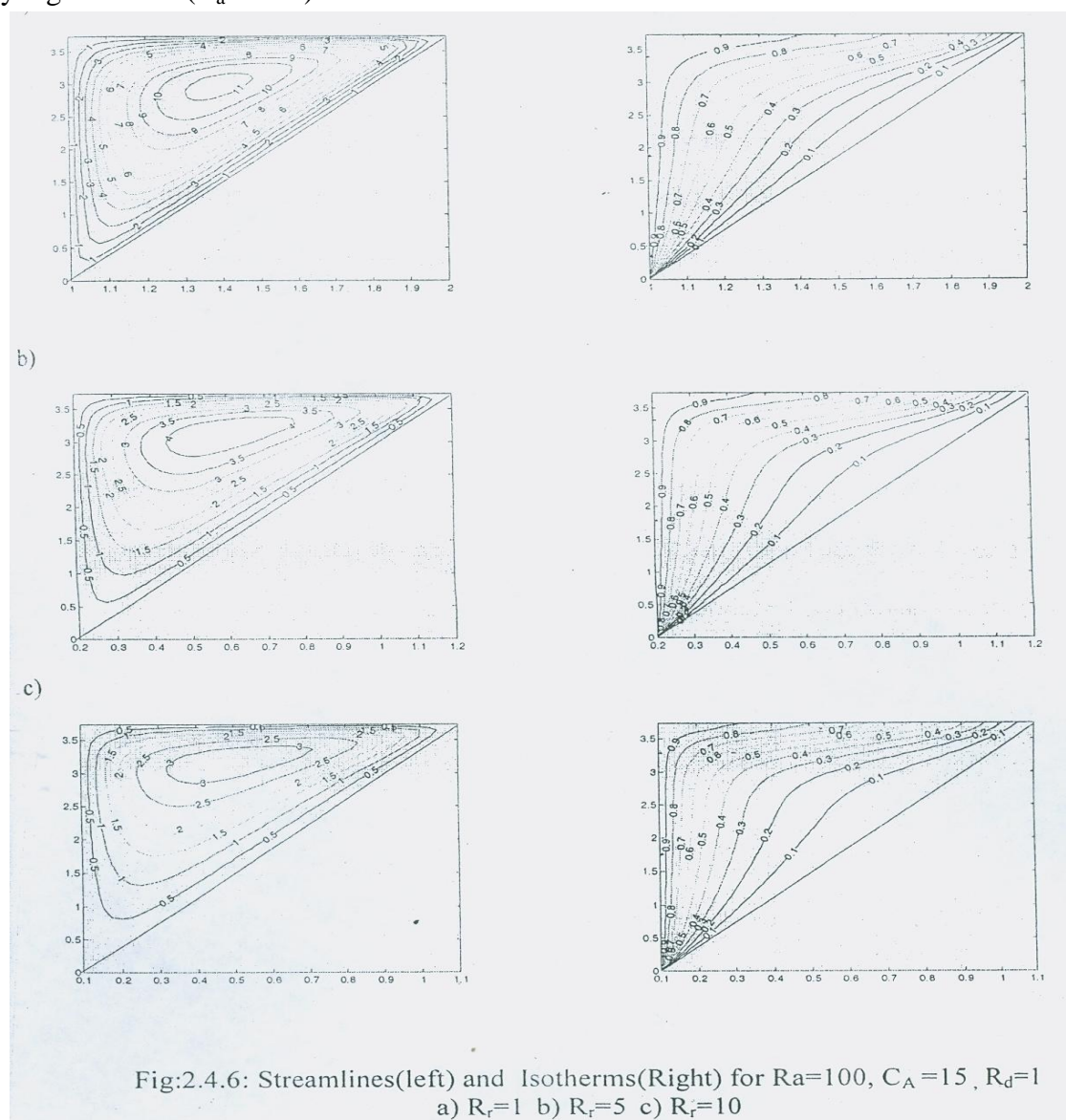
Fig (4.7) illustrates the variation of the average Nusselt number ($\overline{Nu}$) at hot wall, with respect to Radius ratio (R_r) of the vertical annular cone for various values of Cone angles (c_A) at values $R_a = 50$, $R_d = 1$. It is found that the average Nusselt number ($\overline{Nu}$) increases with increase in Radius ratio (R_r). It can be seen that the average Nusselt number ($\overline{Nu}$) increases with increase in Cone angle (c_A). For a given Radius ratio (R_r), the difference between the average Nusselt number ($\overline{Nu}$) for two difference values of Cone Angle (c_A) increased with increase in Cone angle (c_A). For instance, the average Nusselt number ($\overline{Nu}$) increased 11.4%, when Cone angle (c_A) is increased 15 to 45, at $R_r = 1$. However the average Nusselt number ($\overline{Nu}$) increased 6.6% when cone angle is increased 15 to 45 at $R_r = 10$. This difference becomes more as the Radius Ratio (R_r) increase.

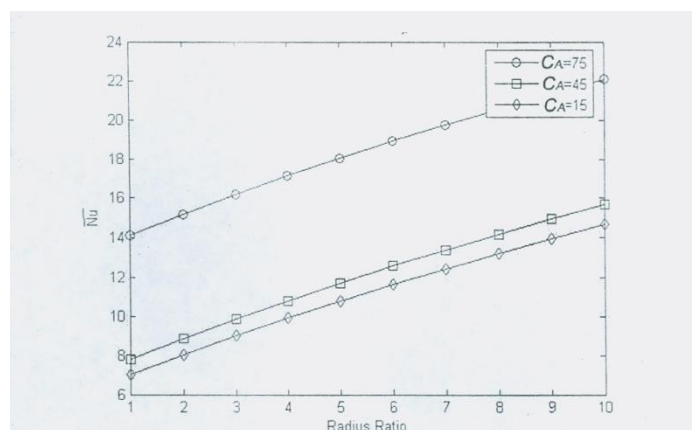Fig.2.4.7: $\bar{N}u$ variations with R_r at hot surface for different values of C_A at Ra=50, R_d=1
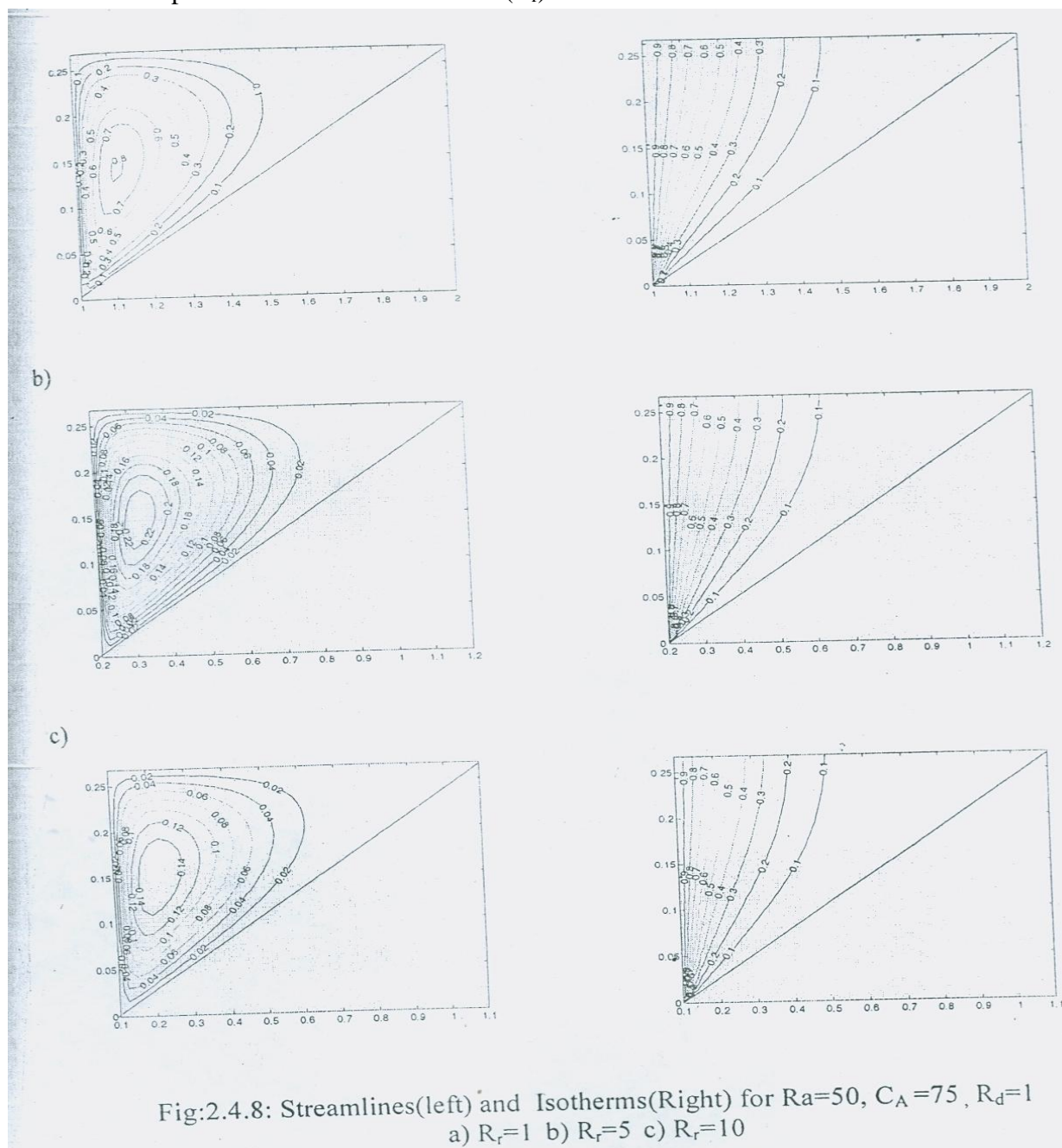
Fig (4.8) represents the streamlines and isothermal lines for various values of Radius ratio (R_r) at R_a = 50, c_A = 75 and R_r = 1. It is clear from the streamlines and isothermal lines that the thermal boundary layer thickness decreases as the Radius ratio (R_r) increases. The magnitude of the streamlines increases as Radius ratio (R_r) increases and tends to move towards the cold wall of the vertical annular cone. At low Radius ratio (R_r) the streamlines tend to occupy the half domain of the vertical annular cone as compared to the higher value, of Radius ratio (R_r). It is clearly seen that more convection heat transfer take place as the upper portion of the vertical annular cone. The streamlines and isothermal lines shifts from the left upper portion of the hot wall to the upper portion of the cold wall of vertical annular cone as the Radius ratio (R_r) increases.

Fig (4.9) represents the streamlines and isothermal lines for various values of Radius ratio (R_r) at R_a = 100, c_A = 75 and R_d = 1. Almost connecting for Fig.4.8 will hold good here also.

Fig (4.10) shows the variation of average Nusselt number ($\bar{N}u$) at hot wall, with respect to Rayleigh number (R_a) of the vertical annular cone for various values of Cone angle (c_A) at R_a = 100, R_d = 1. It is found that the average Nusselt number ($\bar{N}u$) increases with increase in Radius ratio (R_r). It can be seen that the average Nusselt number ($\bar{N}u$) increase with increase in Cone angle (c_A). For a given Radius ratio (R_r) the difference between the average Nusselt number ($\bar{N}u$) increase 11.8%, when Cone angle (c_A). 15 to 45 at Rr = 1. However the average Nusselt number ($\bar{N}u$) increased 6.2% when Cone angle (c_A) is increased 15 to 45 at R_r = 10. This difference becomes more prominent as the Radius ratio (R_r) increase. The average Nusselt number ($\bar{N}u$) increases substantially when the Cone angle (c_A) increased for 45^0 to 75^0.

Fig (4.11) depicts the average Nusselt number ($\bar{N}u$) at hot wall with respect to Radius ratio (R_r), for various values of Radiation parameter (R_d). This figure corresponds to the values R_a = 50, c_A = 75. It is found that the average Nusselt number ($\bar{N}u$) increases with increase in Radius ratio (R_r). It can also be seen that the average Nusselt number ($\bar{N}u$) increases with increase in Radiation parameter (R_d). For a given Radius ratio (R_r), the difference between the average Nusselt number ($\bar{N}u$) increased by 128%, when Radiation parameter (R_d) is increased form 1 to 5, at R_r = 1. However the average Nusselt number ($\bar{N}u$) increased by

159%, when Radiation parameter (R_d) is increased from 1 to 5, at $R_r = 10$. This difference becomes more prominent as the Radius ratio (R_r) increase.
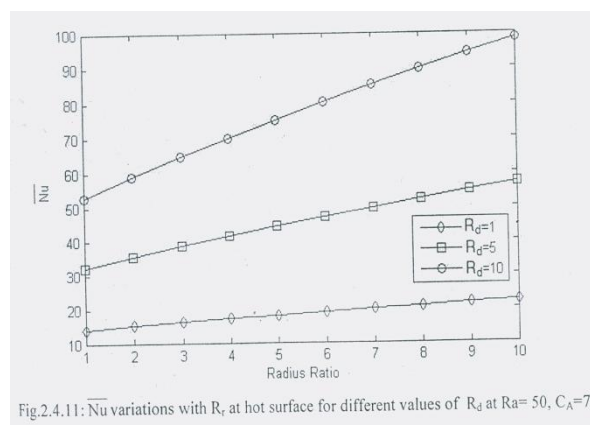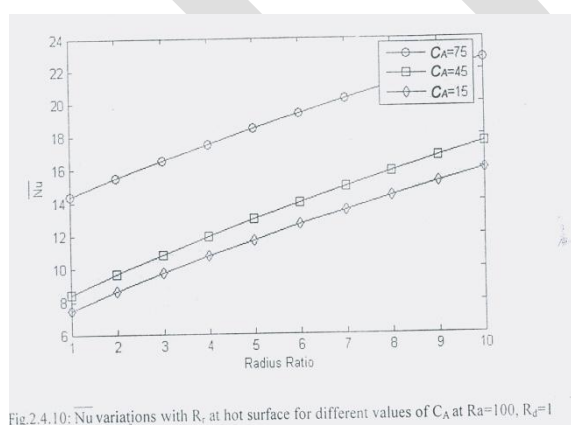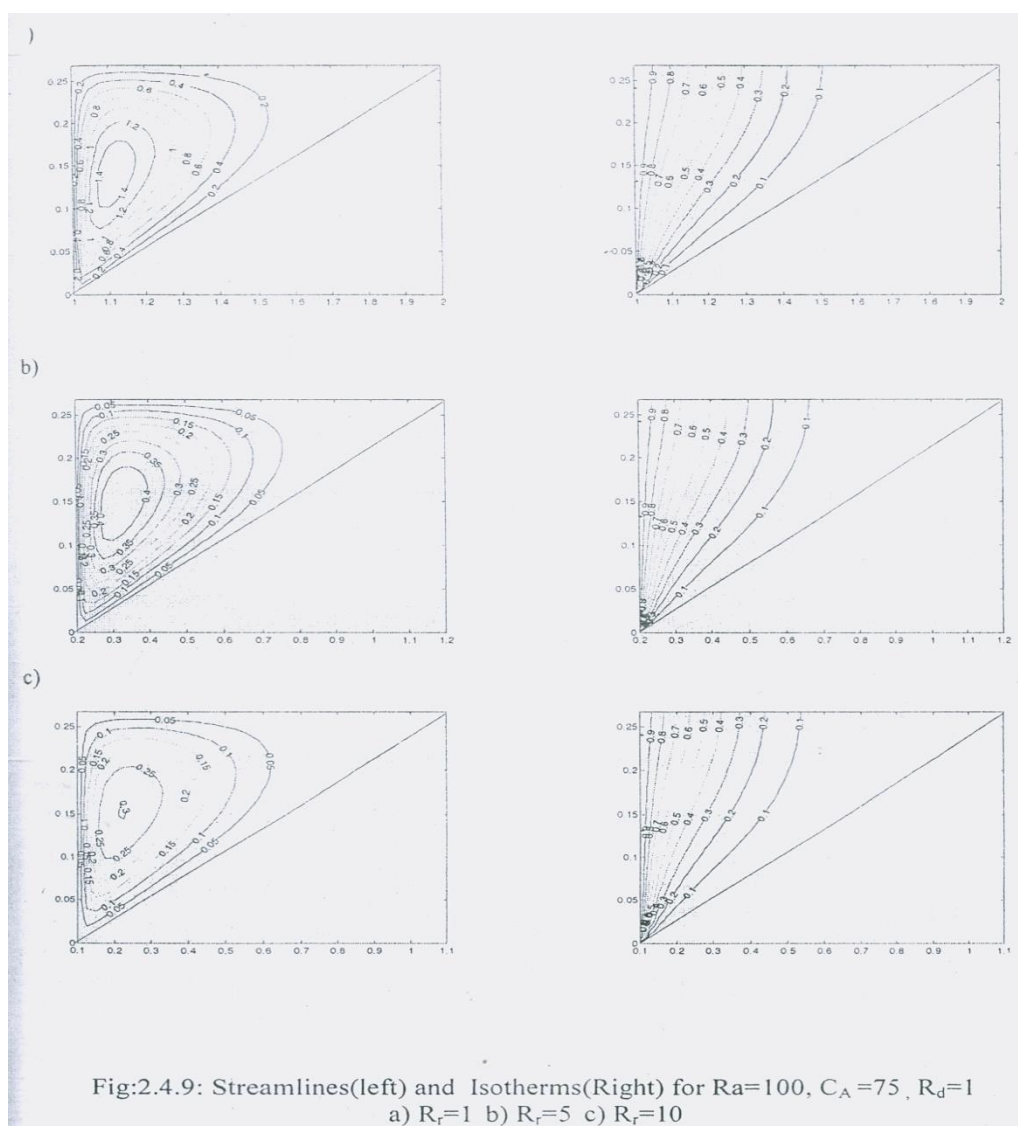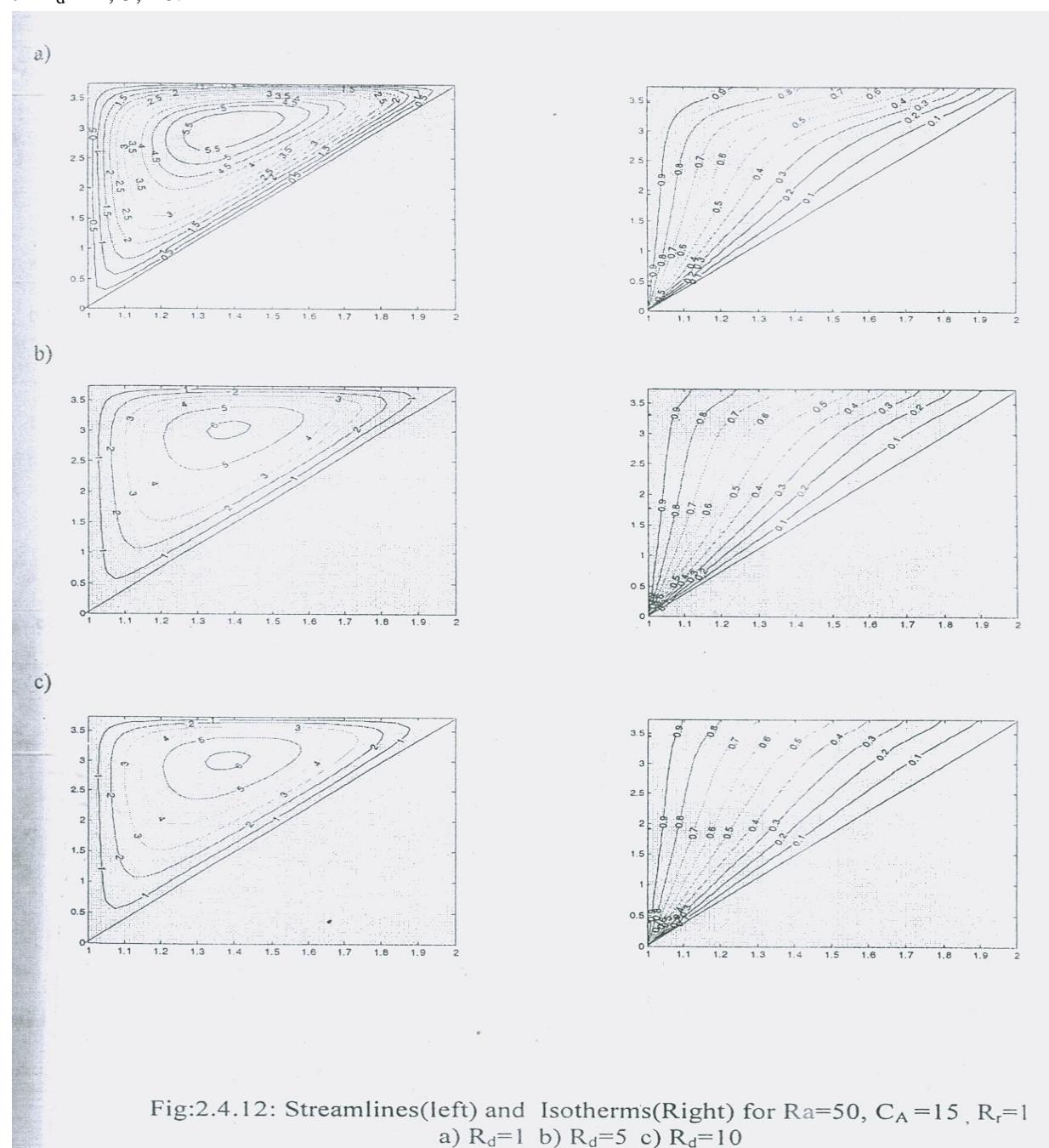

Fig:2.4.8: Streamlines(left) and Isotherms(Right) for Ra=50, C_A =75 , R_d=1
a) R_r=1 b) R_r=5 c) R_r=10

Fig:2.4.9: Streamlines(left) and Isotherms(Right) for Ra=100, C_A =75, R_d=1
a) R_r=1 b) R_r=5 c) R_r=10

Fig.2.4.10: $\overline{Nu}$ variations with R_r at hot surface for different values of C_A at Ra=100, R_d=1

Fig.2.4.11: $\overline{Nu}$ variations with R_r at hot surface for different values of R_d at Ra= 50, C_A=75

Fig (4.12) shows the streamlines and isothermal lines inside the porous medium for various values of Radiation parameter (R_d) at R_a = 50, c_A = 15 and R_r = 1. For the increase of values of the Radiation parameter (R_d) the boundary layer thickness decreases. The streamlines and isothermal lines tend to occupy the whole domain of the vertical annular cone.

Fig (4.13) shows the streamlines and isothermal lines inside the porous medium for various value of Radiation parameter (R_d) at $R_a = 100$, $c_A = 15$ and $R_r = 1$. It can be observed that there is not much change in streamlines in increases when Ra changes for 50 to 100.

Fig (4.14) shows the variation of average Nusselt number ($\overline{N}u$) at hot wall, with respect to Radius ratio (R_r) of the vertical annular cone for various values of Radiation parameter (R_d). This figure corresponds to the values $R_a = 100$, $c_A = 75$. It can be observed from Fig 2.14 that the increase of R_a from 50 to 100 has a small effect in the presence of the radiation for values of $R_d = 1, 5, 10$.
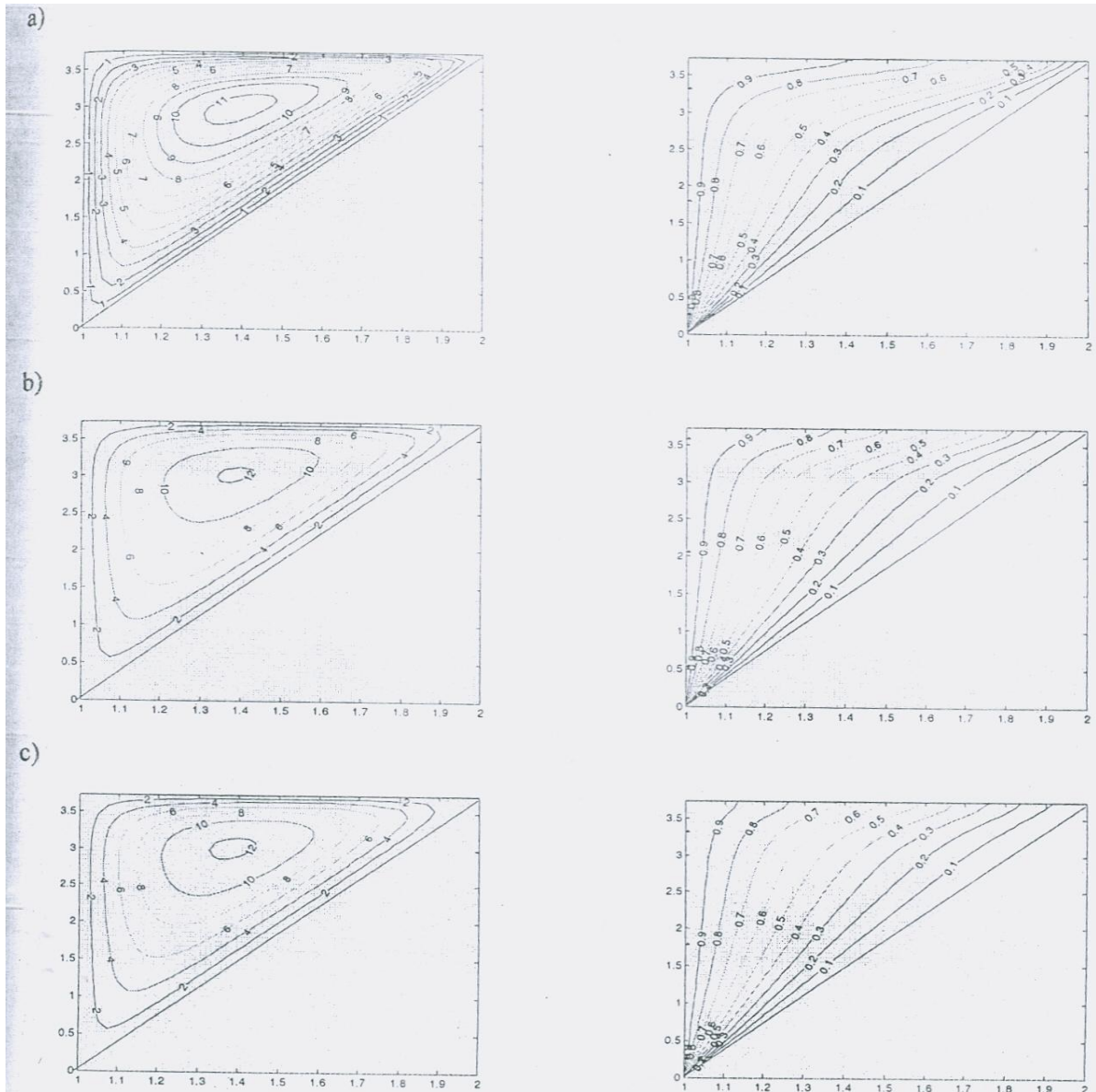

Fig:2.4.12: Streamlines(left) and Isotherms(Right) for Ra=50, C_A=15, R_r=1
a) R_d=1 b) R_d=5 c) R_d=10

Fig:2.4.13: Streamlines(left) and Isotherms(Right) for Ra=100, C_A =15 , R_r=1
a) R_d=1 b) R_d=5 c) R_d=10

Fig (4.15) illustrates the variation of average Nusselt number ($\overline{Nu}$) at hot wall, with respect to Radius ratio (R_r) of the vertical annular cone for various values of Cone angle (c_A) Rayleigh number (R_a) at values R_d = 1, c_A = 75. It is found that the average Nusselt number ($\overline{Nu}$) at R_r = 1 is increased by 1.4%. The corresponding increase in average Nusselt number ($\overline{Nu}$) at R_r = 10 is found to be 2.7%. This is due to the reason that high Rayleigh number (R_a) produces high buoyancy force, which leads to increases fluid movements and thus increased the average Nusselt number ($\overline{Nu}$). For a given Radius ratio (R_r) increase in Ra variation increase in average Nusselt number ($\overline{Nu}$) with very little effect from R_a = 25 to 50 and the effect increases marginally for R_a = 75 to 100.

The porous medium for various values of Radiation parameter (R_d). This figure corresponds R_a = 50, c_A = 75 and R_r = 1. For the increase of the values of Radiation parameter (R_d) the

formation of the streamlines and isothermal lines with these values increases. The streamlines and isothermal lines tend to occupy the major part of the domain from hot wall to cold wall.
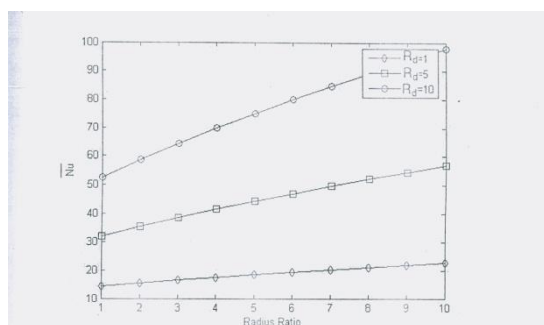

Fig.2.4.14: $\overline{Nu}$ variations with R_r at hot surface for different values of R_d at Ra=100, C_A=75
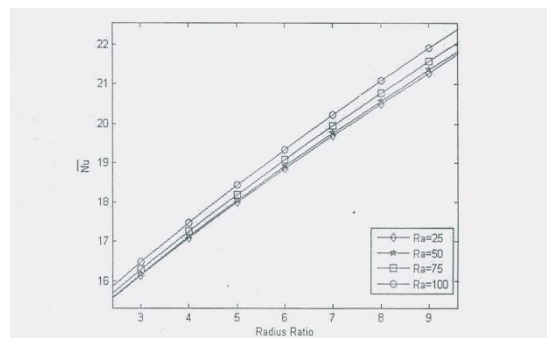
Fig.2.4.15: $\overline{Nu}$ variations with R_r at hot surface for different values of Ra at R_d = 1, C_A= 75

Fig:2.4.16: Streamlines(left) and Isotherms(Right) for Ra=50, C_A =75 , R_r=1
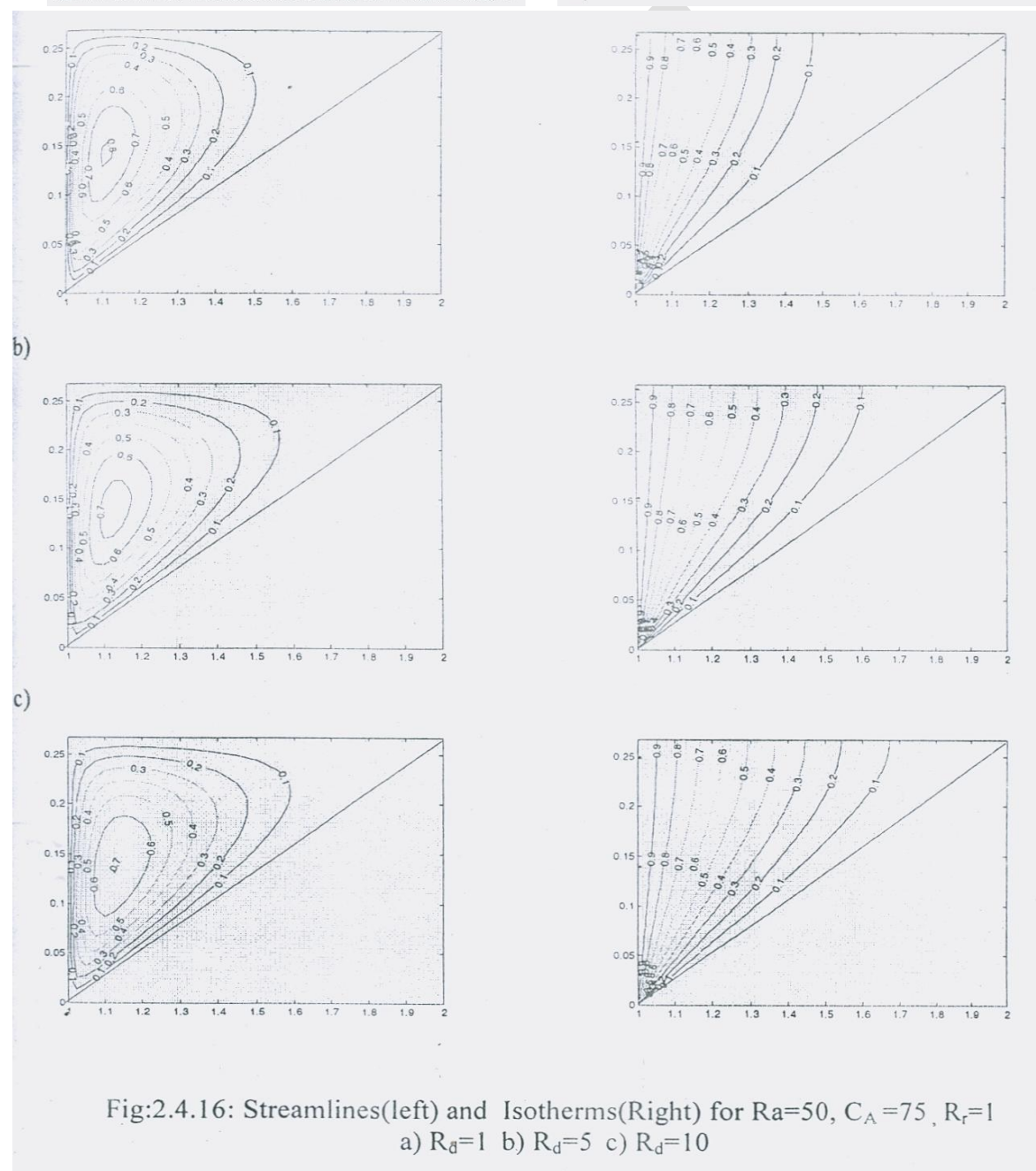a) R_d=1   b) R_d=5   c) R_d=10

Fig:2.4.17: Streamlines(left) and Isotherms(Right) for Ra=100, C_A =75 , R_r=1
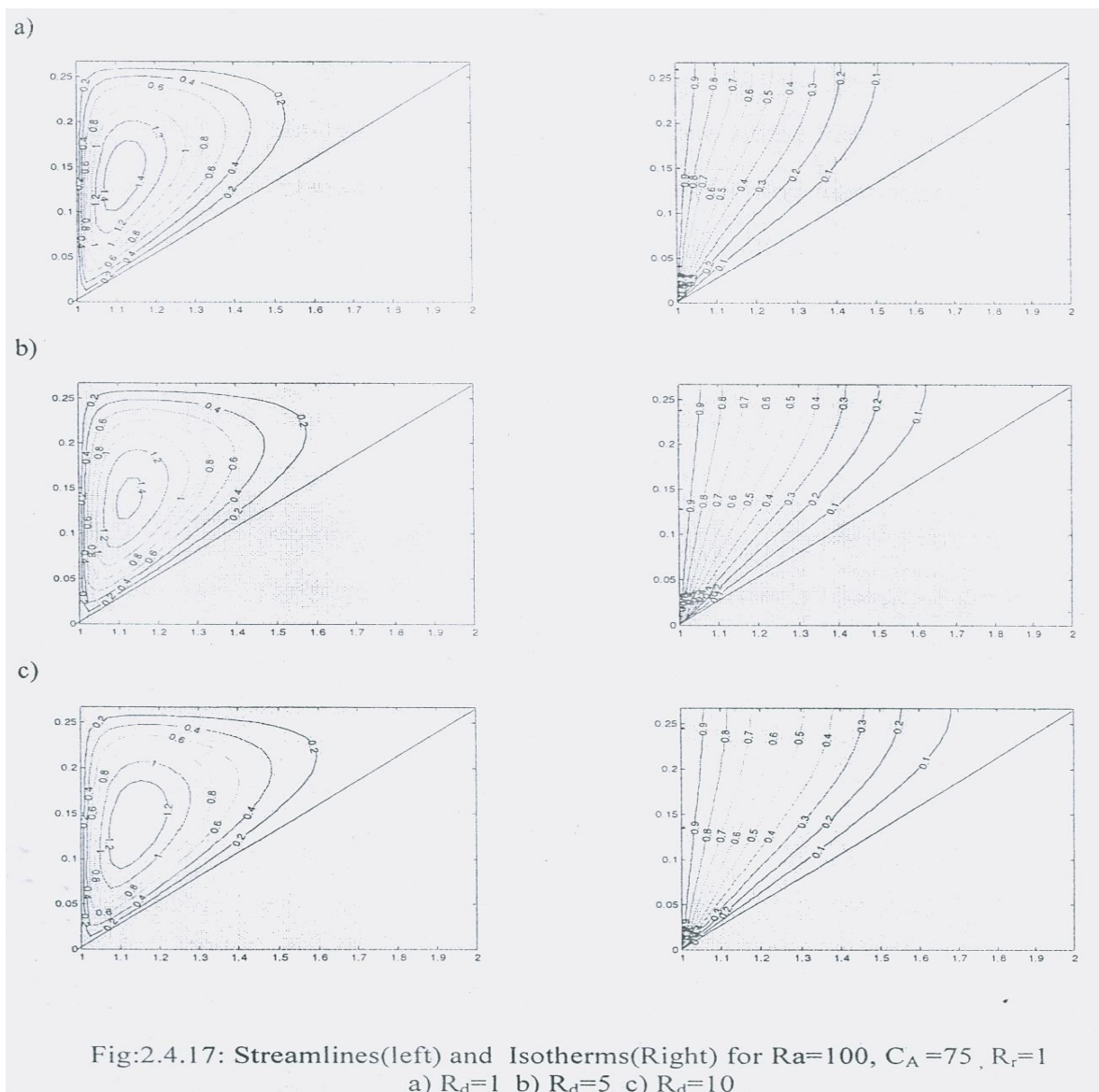a) R_d=1 b) R_d=5 c) R_d=10

Fig (4.17) illustrates the streamlines and isothermal lines distribution inside the porous medium for various value of Radiation parameter (R_d). This figure corresponds to R_a = 100, c_A = 75 and R_r = 1. For the increase of the value of Radiation parameter (R_d) the formation of the streamlines with these values increases. The streamlines and isothermal lines tend to occupy the major part of the domain form hot wall to cold wall. Fig (4.17) is similar to Fig. (4.16) through values vary slightly.

Fig (4.18) shows the variation of average Nusselt number ($\overline{N}u$) at hot wall, with respect to Radiation parameter (R_d) of the vertical annular cone for various values of Cone angle (c_A). This figure corresponds to the values R_r = 1, R_a = 50. It is found that the average Nusselt number ($\overline{N}u$) increases with increase in Radiation parameter (R_d). It can be seen that the average Nusselt number ($\overline{N}u$) increases with increase in Cone angle (c_A). For a given Radiation parameter (R_d), the difference between the average Nusselt number ($\overline{N}u$) at two different values of Cone angle (c_A) increases with increase in Cone angle (c_A). For instance the average Nusselt number ($\overline{N}u$) increased by 12.4% when Cone angle (c_A) is increased from 15 to 45 at R_d = 1. However the average Nusselt number ($\overline{N}u$) increased by 3.1%.

When Cone angle (c_A) is increased from 15 to 45 at $R_d = 10$. The increase in $\overline{Nu}$ for increase of Cone angle (c_A) form 45^0 to 75^0 is substantial. It is interesting to note that the variation of $\overline{Nu}$ with R_d is linear for the three Cone angles (c_A).
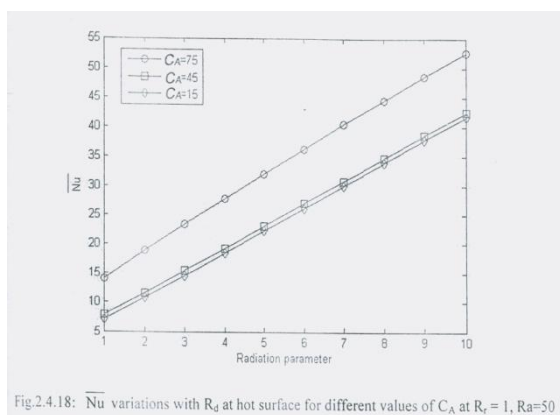

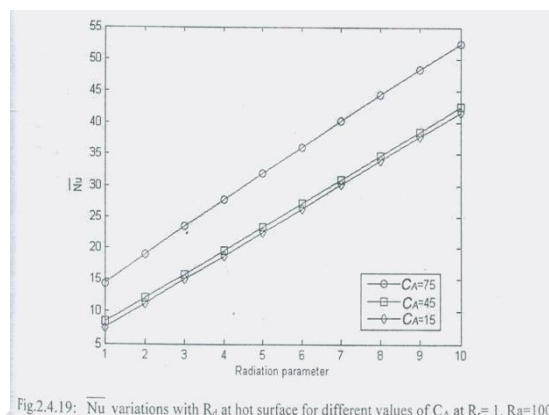Fig.2.4.18: $\overline{Nu}$ variations with R_d at hot surface for different values of C_A at $R_r = 1$, Ra=50   Fig.2.4.19: $\overline{Nu}$ variations with R_d at hot surface for different values of C_A at $R_r = 1$, Ra=100

Fig (4.19) depicts the average Nusselt number ($\overline{Nu}$) at hot wall with respect to Radiation parameter (R_d), for various values of Cone angle (c_A). This figure corresponds to the values $R_r = 1$, $R_a = 100$. Fig (4.19) is very similar to Fig (4.18) and the connects for Fig (4.18) will hold good for Fig. (4.19) also.
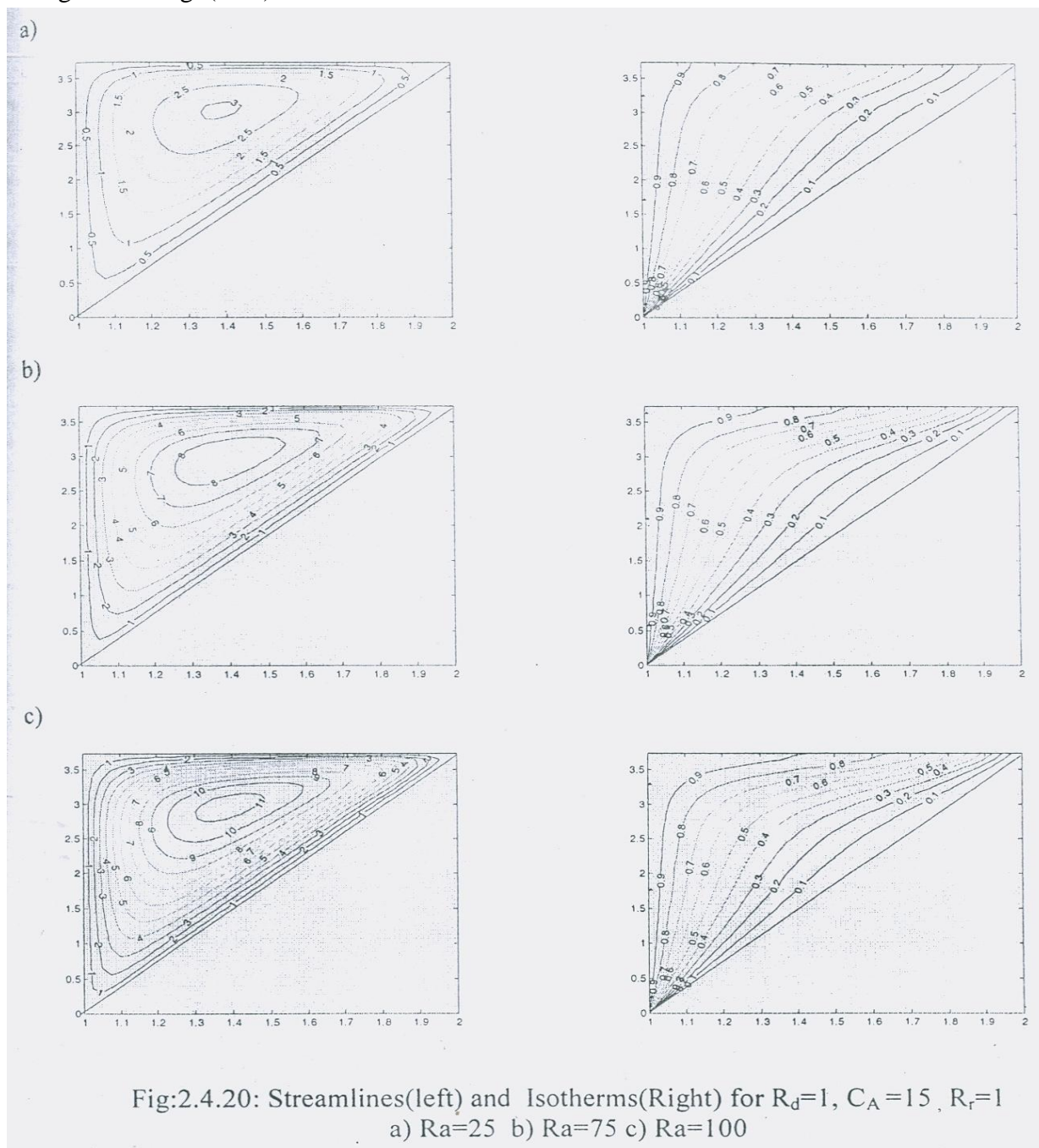
Fig (2.20) shows the streamlines and isothermal lines inside the porous medium for various values of Rayleigh number (R_a) at $R_d = 1$, $c_A = 15$ and $R_r = 1$. The streamlines and isothermal lines tends to move towards the hot wall and away from cold wall of the vertical annular cone as Rayleigh number (R_a) increases. This increase thermal gradient at hot wall and decreases the same at cold wall of the vertical annular cone. Thus heat transfer rate increase at the hot wall and decreases at cold wall with increasing Rayleigh number (R_a). The magnitude of streamlines increases as the Rayleigh number (R_a) increases. The thermal boundary layer becomes thinner as the Rayleigh number (R_a) increase.
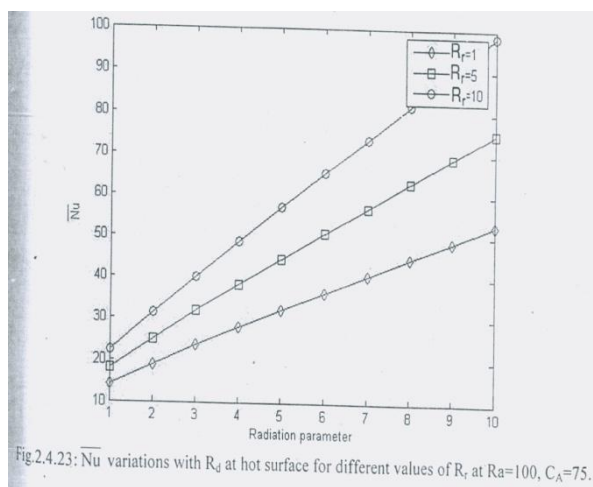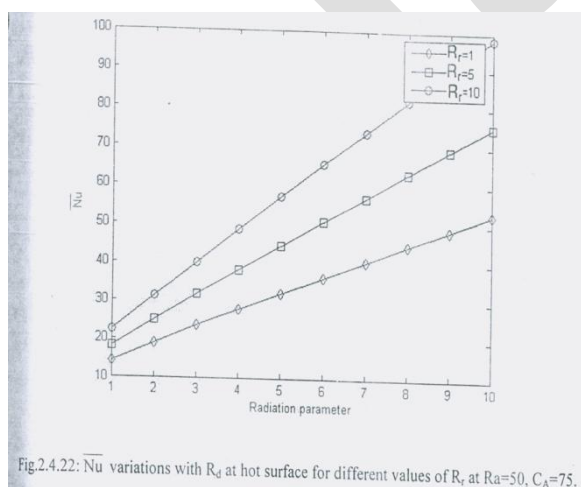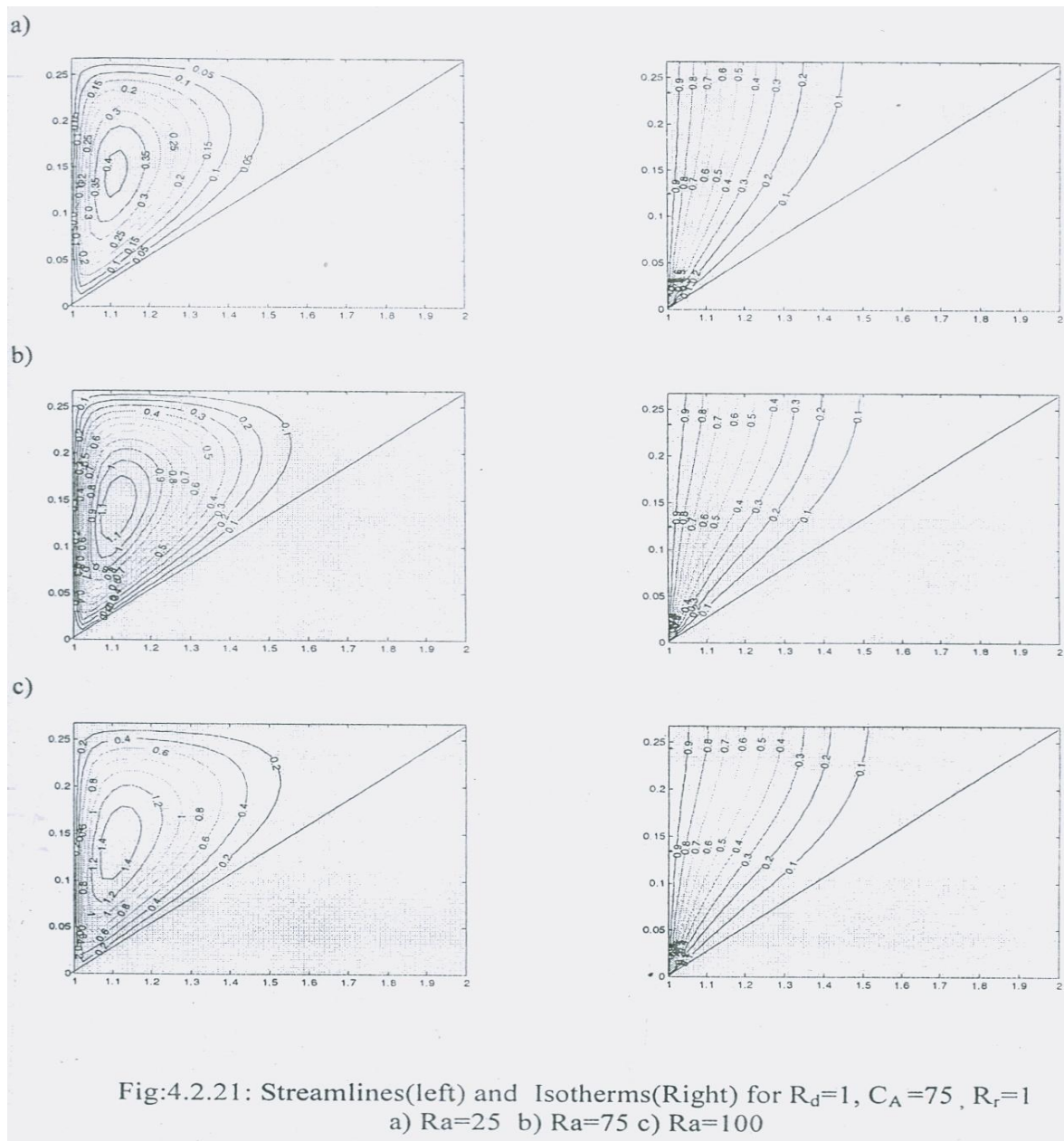
Fig (2.21) illustrates the streamlines and isothermal lines distribution inside the porous medium for various values of Rayleigh number (R_a). This figure corresponds to $R_d = 1$, $c_A = 75$ and $R_r = 1$. It is in clear from the streamlines and isothermal lines that the thermal boundary layer thickness degreases as the Rayleigh number (R_a) increases. The magnitude of the streamlines increase as Rayleigh number (R_a) increase. At low Rayleigh number (R_a) the stream lines tend to occupy the half domain of vertical annular cone as compared to higher value, of Rayleigh number (R_a). It is clearly seen that more convection heat transfer take place at the upper portion of the vertical annular cone.

Fig (4.22) illustrates the variation of average Nusselt number ($\overline{Nu}$) at hot wall, with respect to Radiation parameter (R_d) of the vertical annular cone for various values of Radius ratio (R_r) at values $R_a = 50$, $c_A = 75$. It is found that the average Nusselt number ($\overline{Nu}$) increases with Radiation parameter (R_d) linearly. It can be seen that the average Nusselt number ($\overline{Nu}$) increases with increase in Radius ratio (R_r). For a given Radiation parameter (R_d), the difference between the average Nusselt number ($\overline{Nu}$) at two different values of Radius ratio (R_r) increases with increase in Radius ratio (R_r). For instance, the average Nusselt number ($\overline{Nu}$) increased by 35%, when Radius ratio (R_r) increased from 1 to 5 at $R_d = 1$. However the

average Nusselt number ($\overline{\text{Nu}}$) increased by 48%, when Radius ratio (R_r) is increased from 1 to 5 at R_d = 10. This difference becomes more as the Radiation parameter (R_d) increases. Fig (4.23) depicts the average Nusselt number ($\overline{\text{Nu}}$) at hot wall, with respect to Radiation parameter (R_d) of the vertical annular cone for various values of Radius ratio (R_r) at values R_a = 100, c_A = 75. Fig (4.23) is similar to Fig (4.22) and the connects made for Fig (4.22) will hold good for Fig. (4.23) also.

Fig:2.4.20: Streamlines(left) and Isotherms(Right) for R_d=1, C_A=15 , R_r=1
a) Ra=25 b) Ra=75 c) Ra=100

Fig:4.2.21: Streamlines(left) and Isotherms(Right) for R_d=1, C_A =75 , R_r=1
a) Ra=25 b) Ra=75 c) Ra=100

Fig.2.4.22: $\overline{Nu}$ variations with R_d at hot surface for different values of R_r at Ra=50, C_A=75.

Fig.2.4.23: $\overline{Nu}$ variations with R_d at hot surface for different values of R_r at Ra=100, C_A=75.

5.CONCLUSION

In this paper, we concentrated on the study of heat transfer by free Convection in a saturated porous medium including radiation confined in a vertical conical annular porous medium

6. REFERENCE:

1) P. Cheng and W.J. Minkowyez, J. Geophysics. Res – 82, p 2040 (1977).
2) T.Y. Na and I. Pop, Int. J. Engg. Sci-21, p 517 (1983).
3) R.S.R. Gorla and A.H. Zinalabedini, ASME J. Energy Resources, Technology – 109, p 26 (1987).
4) W.J. Minkowycz and P. Cheng, Int.J. Heat and Mass Transfer – 19, p 805 (1976).
5) A.Yucel, Numerical Heat transfer – 7, p 483 (1984).
6) M. Kumori, I. Pop and G .Nath, Int. J. Heat Mass Transfer-28, p 2171 (1985).
7) J.H. Merkin, Acta Mechanica-62, p 19 (1986).
8) A.P. Bassom and D.A.S. Rees, Acta Mechanica, 116, p 139 (1996).
9) M.A. Hossain and I. Pop, Heat and Mass Transfer, 32, p 223, (1997).
10) A. Raptis, Int. Comm. Heat Mass Transfer, 25, p 289 (1998).
11) P. Cheng, Int. J. Heat and Mass Transfer, 20, p 893 (1997).
12) M. Kazmierezak, D. Poulikakos and I. Pop, Numerical Heat Transfer 10, p 571 (1986).
13) P. Cheng, Adl. Heat Transfer, 14, p 1 (1979).
14) I. A. Hossain, A.Y. Bekeir and R.S.R. Gorla, Heat and Mass Transfer 34, p 209 (1998).
15) R. Viskanta and R.J. Grosh, Int. J. Heat and Mass Transfer 5, p 795 (1962).
16) M.A. Ali, T. Scolen and B.F. Armaly, AIAA. J., 22, p 1797 (1984).
17) A.Y. Bakier and R.S.R. Gorla, Transport in porous media, 23, p 357 (1996).
18) M.A. Hossain and D.A.S. Ress., Acta Mechanica, 127, p 63 (1998).
19) A.Y. Bakeir, Int. Comm. Heat and Mass Transfer, 28 p 119 (2001).
20) A. Bejan, 'Convective Heat Transfer', 2nd edn., New York, John Willey and Som (1995).
21) R.W.Lewis, P. Nithorasu and K.N. Seetharamu, 'Fundamentals of the finite element method for heat and fluid flow' John Wiley and Sons, Chicherter (2004).
22) L.J. Segerland, 'Applied Finite element Analysis', John Willey and Sons, New York (1982).
23) Modeol, M.A. Radiative heat Transfer, New York, McGraw-Hill (1993).